Journal of Materials Chemistry B

ROYAL SOCIETY OF CHEMISTRY

COMMUNICATION

View Article Online
View Journal | View Issue

Cite this: J. Mater. Chem. B, 2024, 12, 8062

Received 5th May 2024,
Accepted 22nd July 2024

DOI: 10.1039/d4tb00960f

rsc.li/materials-b

Enhancing spleen-targeted mRNA delivery with branched biodegradable tails in lipid nanoparticles†

Yupeng Ren,‡[a] Ling Zeng,‡[b] Yingsen Tang,[b] Jing Liao,[b] Meng Jiang,[b] Xinxiu Cao,*[a] Hui Fan*[a] and Jinjin Chen *[b]

The application of mRNA therapy is constrained by the current lipid nanoparticles' (LNPs) inability to target non-liver tissues. In this study, we demonstrate that ionizable lipids equipped with branched and biodegradable tails enhance the selective delivery of mRNA to the spleen, particularly to antigen-presenting cells. This approach offers novel insights into how the chemical structure of LNPs influences their organ-specific targeting capabilities.

[a] *Hunan Provincial Key Laboratory of Advanced Materials for New Energy Storage and Conversion, School of Materials Science and Engineering, Hunan University of Science and Technology, 2 Taoyuan Street, Xiangtan 411201, P. R. China. E-mail: xxcao@hnust.edu.cn, huifan@hnust.edu.cn*

[b] *Guangdong Provincial Key Laboratory of Malignant Tumor Epigenetics and Gene Regulation, Guangdong-Hong Kong Joint Laboratory for RNA Medicine, Medical Research Center, Sun Yat-sen Memorial Hospital, Sun Yat-sen University, Guangzhou 510120, China. E-mail: chenjj365@mail.sysu.edu.cn*

† Electronic supplementary information (ESI) available: The initial *in vivo* screening, the characterization of purified lipids, the size, PDI, and zeta potential of LNPs, and the gating information for flow data. See DOI: **https://doi.org/10.1039/d4tb00960f**

‡ These authors contributed equally.

Jinjin Chen

Dr. Jinjin Chen is currently a principal investigator at the Sun Yat-sen Memorial Hospital, Sun Yat-sen University, where his research team is focused on mRNA delivery and therapy. He received his BS degree in Chemistry from the University of Science and Technology of China. He then obtained his PhD in Polymer Chemistry under the guidance of Prof. Xuesi Chen from Changchun Institute of Applied Chemistry. He completed his postdoctoral fellowship at the Tufts University, working with Prof. Qiaobing Xu.

Since the global administration of mRNA vaccines during the COVID-19 pandemic, mRNA therapy has garnered substantial attention.[1] Currently, LNPs are the sole mRNA carriers authorized by regulatory agencies among various delivery vehicles.[2–4] The COVID-19 mRNA vaccines produced by Moderna and Pfizer/BioNTech, which employ LNPs as carriers, have demonstrated high efficacy and favorable safety profiles.[5] And LNPs offer promising applications for the diagnosis and treatment of viral hepatitis and cancer through integration with CRISPR/Cas gene editing.[6–8] However, LNPs predominantly target liver tissues following both intravenous and intramuscular administrations.[9] This liver-specific delivery not only heightens the risk of hepatotoxicity but also restricts the potential applications of mRNA therapy for non-hepatic diseases. Consequently, developing LNP materials for targeted transfection of specific tissues, organs, or cells will be a future direction in the development of RNA therapeutics.[10,11]

A typical LNP comprises cationic or ionizable lipids, cholesterol, helper lipids, and PEGylated lipids. Given that cationic or ionizable lipids are crucial components of LNPs, their chemical structures significantly influence the efficiency and specificity of mRNA delivery.[12] An ionizable lipid typically consists of a head, a linker, and a tail. In prior research, our group demonstrated that non-hepatic delivery of mRNA could be achieved by optimizing the lipid heads and linkers. For example, an amine head featuring an imidazole group facilitated spleen-specific mRNA delivery, while an amide linker promoted lung-specific mRNA expression.[13–15] However, reports on the non-hepatic delivery of mRNA that leverage the diversity of tail structures remain scarce, thereby limiting a comprehensive understanding of the relationship between the chemical structure of LNPs and their organ-targeting capabilities.

In this study, we synthesized a novel library of ionizable lipids featuring various combinations of heads and tails. The library construction involved a two-step reaction process, as illustrated in Fig. 1. Initially, tails were synthesized *via* the esterification of a brominated spacer with either a branched or

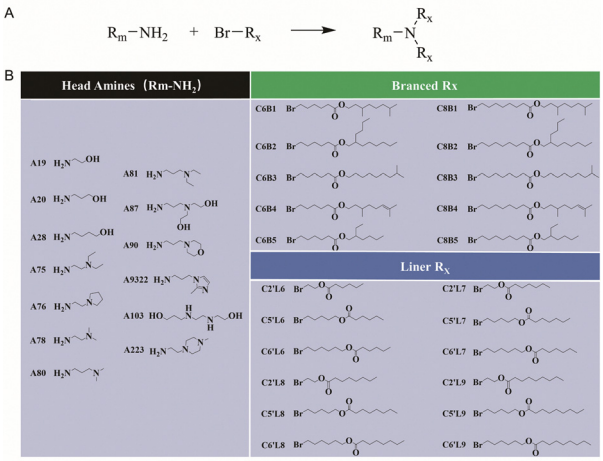

Fig. 1 Methods for constructing a lipid library. (A) Reaction mechanisms of the amine and brominated tails. (B) Structures of the amine and brominated tails used in the synthesis of a library.

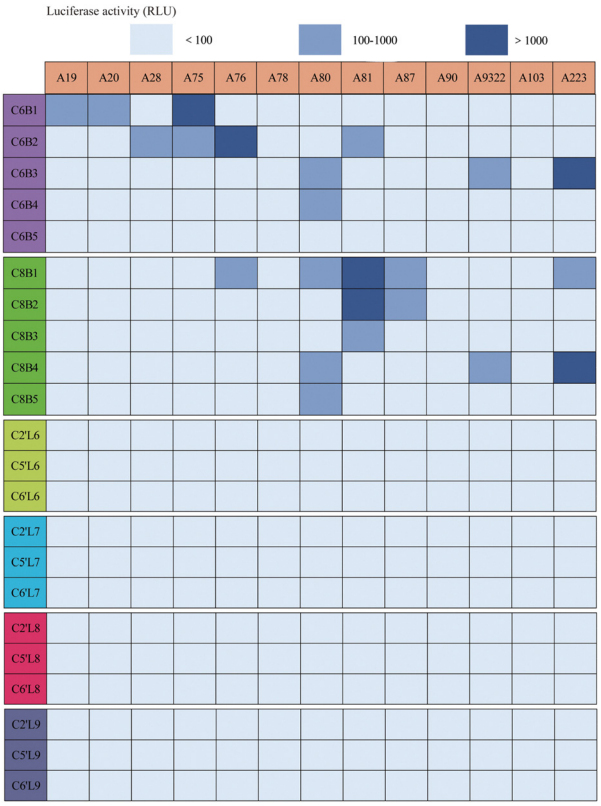

Fig. 2 The luciferase intensity in HeLa cells after treatment with mLuc-loaded LNPs for 24 h.

a linear end group. Subsequently, these tails (Fig. S1, ESI†) were reacted with different amine heads, resulting in a comprehensive library of 286 distinct lipid structures. The tails consisted of carbon spacers and alkyl chains, which varied in length, branching, and saturation, all linked by a biodegradable ester bond. The lipids were designated as A*x*C*y*B*z* for those with branched tails, and A*x*C*y*L*z* for those with linear tails, as depicted in Fig. 1B.

For the initial screening, LNPs were assembled using crude lipids, cholesterol, distearoylphosphatidylcholine (DSPC), and 1,2-dicarnosine-sr-3-methoxy (polyethylene glycol)2000 (DMG-PEG2000) in a mass ratio of 16 : 4 : 2 : 1. Firefly luciferase mRNA (mLuc) served as the reporter mRNA, incorporated into LNPs at a weight ratio of 20 : 1. The efficacy of mRNA delivery was assessed by measuring luciferase protein expression in HeLa cells post 24-hour incubation with various LNP/mLuc complexes. As depicted in Fig. 2, the initial screening of the 286 LNPs indicated that the tail branching significantly impacted mRNA expression levels. LNPs formulated with branched tail lipids exhibited superior mRNA delivery compared to those with linear tails. The nature of the amine heads also influenced mRNA expression, with amines A19, A20, A28, A75, A76, A80, A81, A9322, and A223 demonstrating more robust signals than other amines. Notably, tails with branched structures B1 and B2 yielded the highest rates of positive mRNA expression. These findings underscore the critical role of branched tail structures in enhancing *in vitro* mRNA expression.

Twenty-three LNPs demonstrating positive *in vitro* mRNA expression were selected for subsequent *in vivo* evaluation. These LNPs, loaded with mLuc, were intravenously injected into 4-week-old ICR mice at a dosage of 2 μg mRNA per mouse. Six hours post-injection, mLuc expression was assessed using an *in vivo* imaging system (IVIS). As illustrated in Fig. S2A (ESI†), lipids with a six-carbon spacer facilitated enhanced whole-body mRNA expression compared to those with an eight-carbon spacer. Consistent with *in vitro* results, lipids with branched tails containing B1 and B2 alkyl chains exhibited higher signals relative to other branched configurations. Key organs, including the heart, liver, spleen, lung, and kidneys, were isolated and imaged to further evaluate the organ specificity of these LNPs (Fig. S2B, ESI†). Predominantly, the lipids demonstrated spleen-specific mRNA expression. Interestingly, the amine head A223 was associated with lung-selective mRNA expression (Fig. S3, ESI†). Notably, the *in vivo* expression patterns were not always consistent with *in vitro* findings. For example, the lipids A76-C6B2 and A81-C8B1, which were highly effective *in vitro*, exhibited negligible signals in mice. This discrepancy could be attributed to the more complex biological conditions encountered *in vivo*.

The five top-performing lipids with high *in vivo* mRNA expression underwent further purification and detailed characterization, employing techniques such as mass spectrometry and ^{1}H NMR, as shown in Fig. S4 (ESI†). Subsequently, LNPs formulated with these purified lipids were analyzed for their size and zeta potential (Fig. S5, ESI†). Dynamic light scattering (DLS) measurements indicated that the hydrodynamic diameters (Dh) of the unloaded LNPs ranged from 100 to 135 nm, with polydispersity indices (PDIs) between 0.15 and 0.25, as depicted in Fig. S5A (ESI†). Upon incorporation of mRNA, the LNPs/mRNA complexes exhibited an increased Dh, ranging from 145 to 200 nm, and displayed narrower PDIs, between 0.09 and 0.20, compared to the blank vehicles. Predictably, the zeta potential of the LNPs shifted from a positive charge towards a nearly neutral

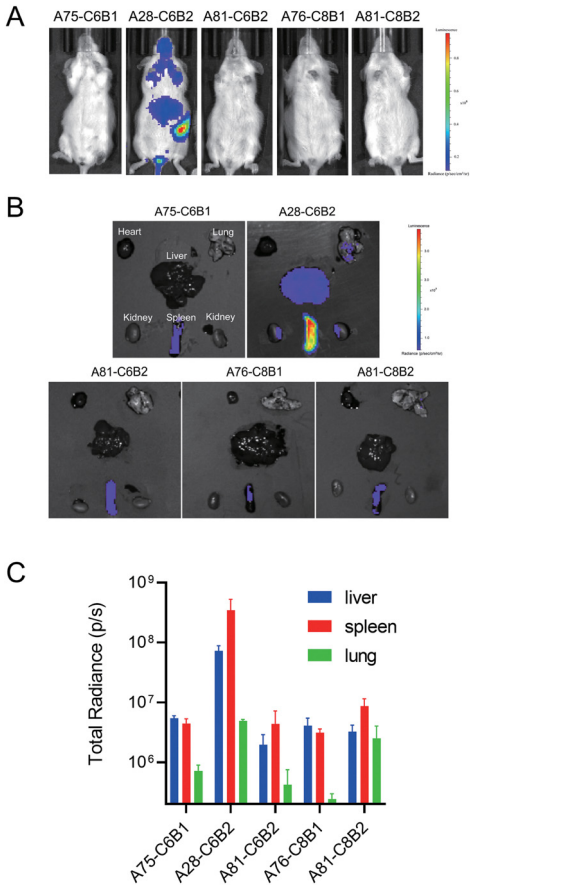

Fig. 3 (A) Representative IVIS images of mice at 6 h post intravenous injection of LNPs (2 μg of mLuc per mouse). (B) *Ex vivo* images of major organs from mice treated with LNPs. (C) Quantification of mRNA expression by five LNPs in various organs.

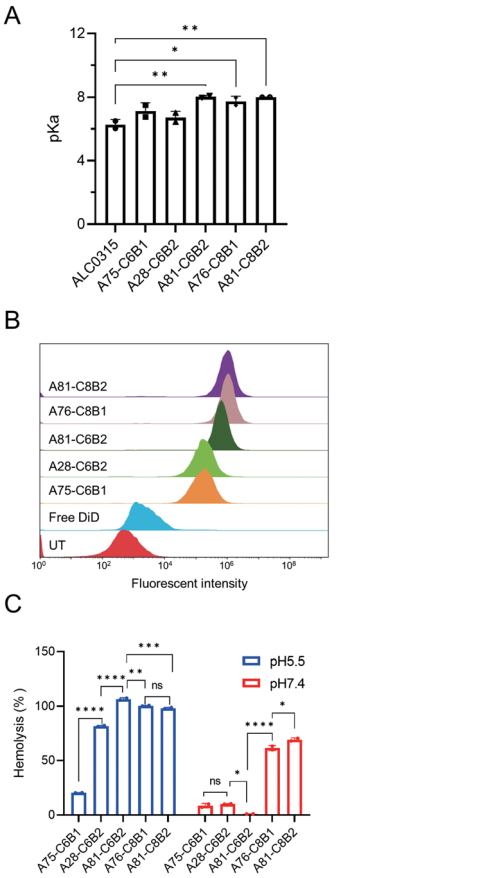

Fig. 4 The pK_a (A), cellular uptake (B), and hemolysis ability (C) of LNPs. Data were presented as mean ± s.d., n = 2. The statistical significance was calculated by one-way ANOVA: *p < 0.05, **p < 0.01, ***p < 0.001, ****p < 0.0001, and ns represents not statistically significant.

charge following mRNA encapsulation, as observed at pH 7.4, according to Fig. S5B (ESI†).

The purified lipids exhibited significant differences in mRNA expression compared to their unpurified counterparts *in vivo* (Fig. 3). All the lipids exhibited spleen-selective mRNA expression (Fig. 3B). Notably, lipid A28-C6B2 demonstrated the highest mRNA expression in the spleen, accounting for ~83% intensity of the whole-body signal. Although other purified lipids also showed targeted mRNA delivery to the spleen to some extent, the expression levels were markedly lower compared to those of the crude lipids. This suggests that certain impurities in the crude products may enhance mRNA delivery under some conditions.

A successful mRNA delivery system must navigate several critical steps: (1) reduced clearance during circulation; (2) substantial accumulation at the target organ; (3) efficient cellular uptake by the targeted cells; and (4) rapid escape from the endosome to the cytoplasm.[16] To investigate how these factors influence mRNA delivery efficacy, we assessed the pK_a, cellular uptake, membrane permeability, biodistribution, and subcellular mRNA expression of these LNPs.

Firstly, the effectiveness of LNPs is largely dependent on their pK_a values.[17] We next tested the pK_a of all LNPs using a 6-(*p*-toluidino)-2-naphthalenesulfonic acid sodium salt (TNS) assay according to a previously published protocol (Fig. S6, ESI†). ALC0315, the gold standard lipid used in COMIRNATY®, was used for comparison, with a pK_a of 6.03, aligning with previously published results. As shown in Fig. 4A, the pK_a of A28-C6B2 was determined to be 6.43, closely matching that of ALC-0315. However, other LNPs displayed significantly higher pK_a values, ranging from 6.68 to as high as 8.0. These findings indicate that pK_a values are primarily influenced by the head structure. For instance, A81, regardless of the tail variations, showed consistent pK_a values, while the difference between lipids A28-C6B2 and A81-C6B2 was approximately 1.5.

The cellular uptake of LNPs was observed to correlate strongly with their pK_a values (Fig. 4B). During experiments conducted at pH 7.4, LNPs with lower pK_a values showed reduced cellular uptake, while those with higher pK_a values demonstrated increased cellular internalization. This variance can be attributed to the higher protonation rate of the tertiary amines at pH 7.4 in LNPs with higher pK_a values, confirming that LNP cellular uptake is determined by their surface charge.[18,19]

Additionally, the hemolytic properties of these LNPs at pH 7.4 and 5.5 were measured to assess their membrane

permeability under different conditions. Ideally, LNPs should exhibit low cell membrane permeability at the physiological pH of approximately 7.4, and high endosomal disrupting capability at the acidic pH of about 5.5.[4] Interestingly, LNPs displayed varying degrees of membrane permeability. Lipids with six-carbon spacers showed negligible hemolysis at pH 7.4, while those with eight-carbon spacers exhibited significant hemolysis, exceeding 50%. As the pH decreased to 5.5, increased protonation of the tertiary amines led to enhanced interaction with cell membranes due to electrostatic interactions. This increased membrane permeability under acidic conditions facilitates the endosomal escape of LNPs and the subsequent release of mRNA into the cytoplasm.[20] These findings suggest that LNP membrane permeability is influenced by both the head amine and the tail structures.

Different from the small molecules, the successful mRNA expression is not equal to the biodistribution. The relationship between the subcellular biodistribution and mRNA expression was evaluated using IVIS and flow cytometry. LNPs were initially incorporated with DiD dye, which indicates the biodistribution of LNPs. mRNA expression was analyzed in a Cre recombinase/LoxP reporter mouse model. When the mRNA encoding Cre mRNA (mCre) is delivered and expressed in cells, the LoxP gene is cut.[21] Subsequently, the tdTomato gene is activated and the protein is expressed with red fluorescence, which can be detected by IVIS and flow cytometry (Fig. S7 and S8, ESI†). The Lipids A28-C6B2 and A81-C8B2 served as positive and negative controls, respectively. As shown in Fig. 5A and D, lipid A28-C6B2 demonstrated an increased DiD and tdTomato signal in the spleen compared to A81-C8B2 and untreated mice. However, both A28-C6B2 and A81-C8B2 LNPs exhibited a similar subcellular distribution, predominantly within F4/80-positive macrophages and CD11c-positive dendritic cells (DCs). Over 80% of these macrophages and DCs were DiD-positive,

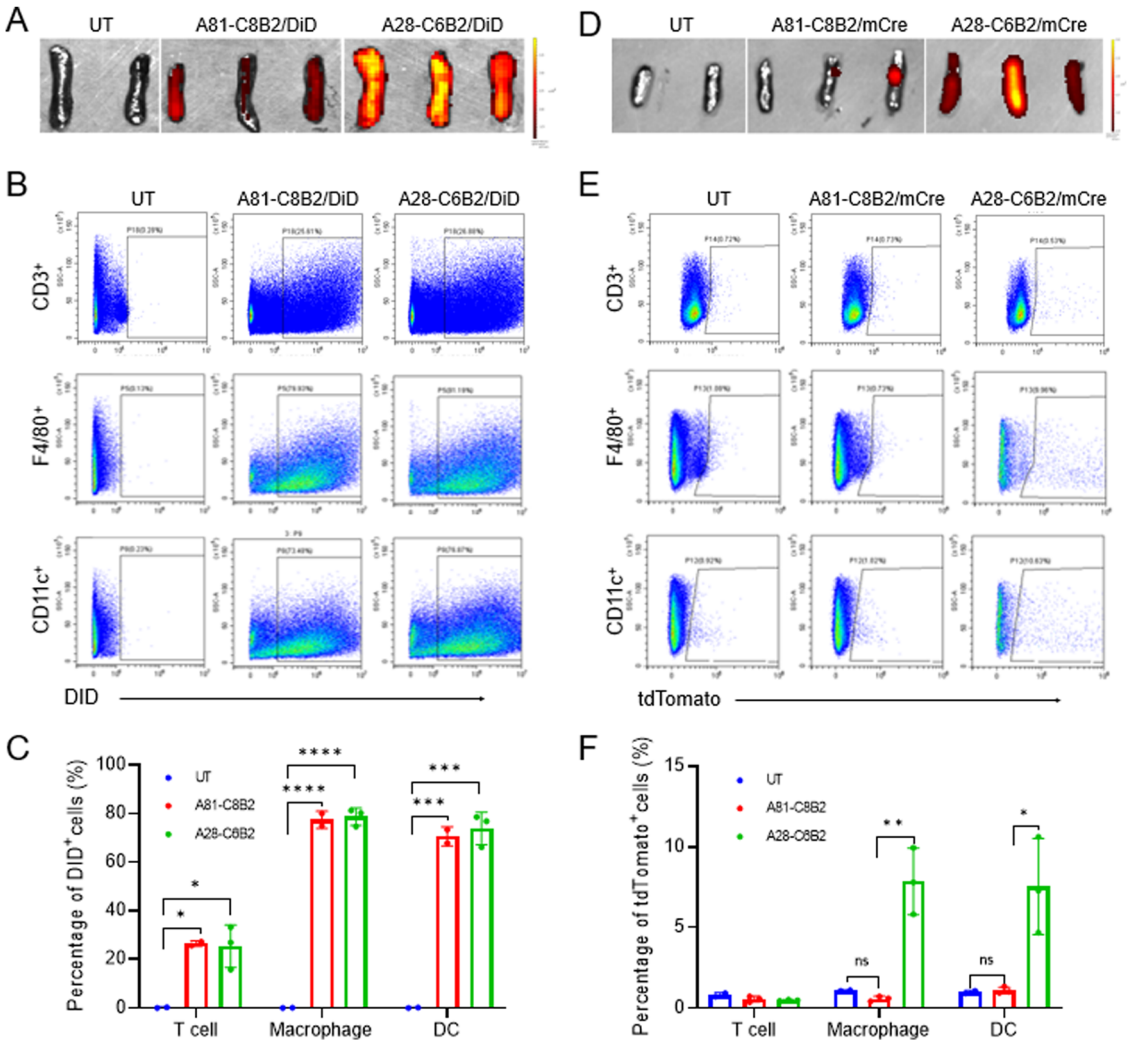

Fig. 5 Biodistribution and mRNA expression of LNPs after I.V. administration. (A) and (D) The IVIS images of spleen after treatment with LNP/DiD (A) and LNP/mCre (D). (B) and (E) The flow cytometry analysis of splenocytes after treatment with LNP/DiD (B) and LNP/mCre (E). (C) and (F) Quantified percentage of DiD-positive (C) and tdTomato-positive (F) splenocytes. Data were presented as mean ± s.d., n = 2–3/group. The statistical significance was calculated by one-way ANOVA: *$p < 0.05$, **$p < 0.01$, ***$p < 0.001$, ****$p < 0.0001$, and ns represents not statistically significant.

significantly higher than that observed in T cells (Fig. 5B and C). Despite this, the percentage of mRNA expression was much lower than the LNP distribution; about 7.5% of macrophages and DCs in the A28-C6B2 group expressed tdTomato protein, while no signal was detected in the A81-C8B2 group (Fig. 5E and F). Moreover, though over 20% of T cells could also take up LNPs, no positive signal of tdTomato expression was detected owing to the difficulty in T cell transfection. The encapsulation efficiency of A28-C6B2 and A81-C8B2 was determined to be 64.15% and 54.15%, respectively, as shown in Fig. S9 (ESI†). The results suggest that the amine head may affect the encapsulation efficiency of LNPs. Although LNPs efficiently delivered mRNA to the correct organs and cells, the expression of mRNA was also influenced by other known or unknown factors.

Conclusions

In this work, we synthesized a new library of ionizable LNPs featuring either branched or linear biodegradable tails. Initial *in vitro* screenings revealed that lipids with branched tails significantly enhanced the efficacy of mRNA delivery compared to those with linear tails. Notably, the lipid A28-C6B2 demonstrated high spleen-specific mRNA expression following intravenous administration. Additionally, A28-C6B2 efficiently targeted mRNA delivery to antigen-presenting cells, underscoring its potential utility in immunotherapy. Interestingly, the specificity of organ-targeted mRNA delivery was influenced not only by the biodistribution of the LNPs but also by factors such as pK_a, cellular uptake, and membrane permeability. This research introduces a novel strategy for non-hepatic mRNA delivery by manipulating tail structures, offering new insights into the interplay between the chemical structures and the targetability of LNPs.

Author contributions

Yupeng Ren: methodology, investigation, data curation, and writing – original draft. Ling Zeng: investigation, data curation, and writing – original draft. Yingsen Tang: investigation and resources. Jing Liao: investigation. Meng Jiang: investigation. Xinxiu Cao: supervision and funding acquisition. Hui Fan: supervision. Jinjin Chen: conceptualization, supervision, writing – review and editing, project administration, and funding acquisition.

Data availability

All relevant data are within the manuscript and the ESI.† The data are available from the corresponding author on reasonable request.

Conflicts of interest

There are no conflicts to declare.

Acknowledgements

We acknowledge the financial support from the National Natural Science Foundation of China (Grant No. 22203028), the Natural Science Foundation of Hunan Province (Grant No. 2024JJ5138), the Fundamental Research Funds for the Central Universities (Grant No. 22hytd12), Guangdong High level Youth Talent Project (Grant No. 2023HYSPT0703), and the grant from Guangzhou Science and Technology Bureau (Grant No. 2024A04J6561).

Notes and references

1 O. Chabanovska, A.-M. Galow, R. David and H. Lemcke, *Adv. Drug Delivery Rev.*, 2021, **179**, 114002.
2 M. Jeong, Y. Lee, J. Park, H. Jung and H. Lee, *Adv. Drug Delivery Rev.*, 2023, 114990.
3 R. Liu, C. Luo, Z. Pang, J. Zhang, S. Ruan, M. Wu, L. Wang, T. Sun, N. Li and L. Han, *Chin. Chem. Lett.*, 2023, **34**, 107518.
4 W. Xiao, F. Wang, Y. Gu, X. He, N. Fan, Q. Zheng, S. Qin, Z. He, Y. Wei and X. Song, *Chin. Chem. Lett.*, 2024, **35**, 108755.
5 E. Fang, X. Liu, M. Li, Z. Zhang, L. Song, B. Zhu, X. Wu, J. Liu, D. Zhao and Y. Li, *Signal Transduction Targeted Ther.*, 2022, **7**, 94.
6 K. Yi, H. Kong, Y. Lao, D. Li, R. Mintz, T. Fang, G. Chen, Y. Tao, M. Li and J. Ding, *Adv. Mater.*, 2024, **36**(13), 2300665.
7 H. Kong, E. Ju, K. Yi, W. Xu, Y. Lao, D. Cheng, Q. Zhang, Y. Tao, M. Li and J. Ding, *Adv. Sci.*, 2021, **8**(24), 2102051.
8 M. Islam, J. Rice, E. Reesor, H. Zope, W. Tao, M. Lim, J. Ding, Y. Chen, D. Aduluso, B. R. Zetter, O. C. Farokhzad and J. Shi, *Biomaterials*, 2021, **266**, 120431.
9 J. Chen, Z. Ye, C. Huang, M. Qiu, D. Song, Y. Li and Q. Xu, *Proc. Natl. Acad. Sci. U. S. A.*, 2022, **119**, e2207841119.
10 T. Wang, T. Sung, T. Yu, H. Lin, Y. Chen, Z. Zhu, J. Gong, J. Pan and A. Higuchi, *J. Mater. Chem. B*, 2023, **11**(23), 5083–5093.
11 D. Loughrey and J. E. Dahlman, *Acc. Chem. Res.*, 2021, **55**, 13–23.
12 H. Ni, M. Z. Hatit, K. Zhao, D. Loughrey, M. P. Lokugamage, H. E. Peck, A. D. Cid, A. Muralidharan, Y. Kim and P. J. Santangelo, *Nat. Commun.*, 2022, **13**, 4766.
13 X. Zhao, J. Chen, M. Qiu, Y. Li, Z. Glass and Q. Xu, *Angew. Chem., Int. Ed.*, 2020, **59**, 20083–20089.
14 M. Qiu, Y. Tang, J. Chen, R. Muriph, Z. Ye, C. Huang, J. Evans, E. P. Henske and Q. Xu, *Proc. Natl. Acad. Sci. U. S. A.*, 2022, **119**, e2116271119.
15 F. Ma, L. Yang, Z. Sun, J. Chen, X. Rui, Z. Glass and Q. Xu, *Sci. Adv.*, 2020, **6**, eabb4429.
16 B. Sun, W. Wu, E. A. Narasipura, Y. Ma, C. Yu, O. S. Fenton and H. Song, *Adv. Drug Delivery Rev.*, 2023, 115042.
17 P. Patel, N. M. Ibrahim and K. Cheng, *Trends Pharmacol. Sci.*, 2021, **42**, 448–460.
18 J. D. Ziebarth and Y. Wang, *Biomacromolecules*, 2010, **11**, 29–38.
19 R. Augustine, A. Hasan, R. Primavera, R. J. Wilson, A. S. Thakor and B. D. Kevadiya, *Mater. Today Commun.*, 2020, **25**, 101692.
20 E. Xu, W. M. Saltzman and A. S. Piotrowski-Daspit, *J. Controlled Release*, 2021, **335**, 465–480.
21 G. Meinke, A. Bohm, J. Hauber, M. T. Pisabarro and F. Buchholz, *Chem. Rev.*, 2016, **116**, 12785–12820.

